Volume 6 | Number 31 | 21 August 2018 | Pages 8269–8558

Journal of Materials Chemistry C

Materials for optical, magnetic and electronic devices

rsc.li/materials-c

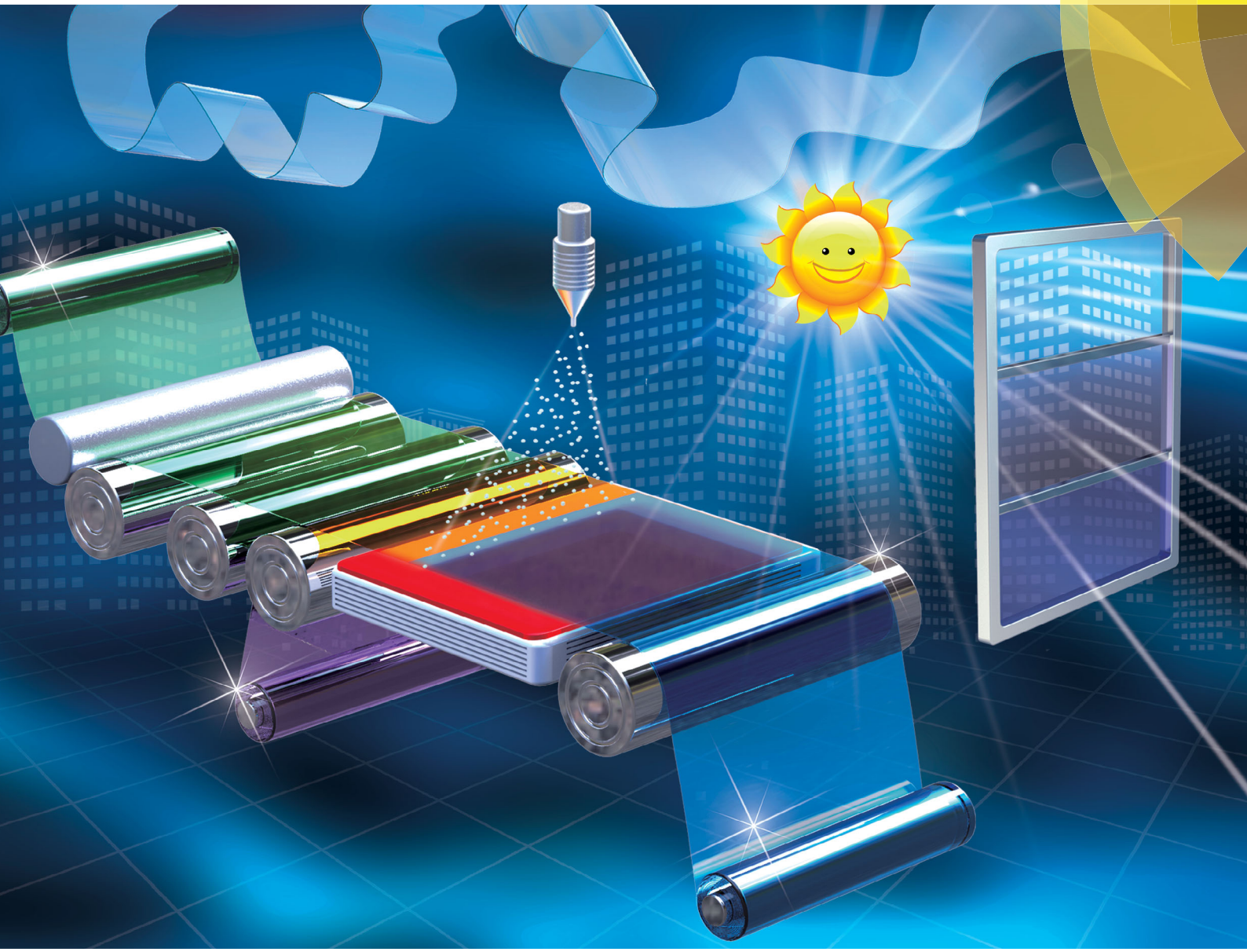

ISSN 2050-7526

ROYAL SOCIETY OF CHEMISTRY

PAPER

Guoqiang Zheng, Chuntai Liu, Zhanhu Guo *et al.*
Continuously fabricated transparent conductive polycarbonate/carbon nanotube nanocomposite films for switchable thermochromic applications

Journal of Materials Chemistry C

PAPER

View Article Online
View Journal | View Issue

Cite this: J. Mater. Chem. C, 2018, 6, 8360

Continuously fabricated transparent conductive polycarbonate/carbon nanotube nanocomposite films for switchable thermochromic applications†

Bing Zhou,[a] Yahong Li,[a] Guoqiang Zheng,*[a] Kui Dai,[a] Chuntai Liu,*[a] Yong Ma,[bc] Jiaoxia Zhang,[bd] Ning Wang,[e] Changyu Shen[a] and Zhanhu Guo*[b]

Received 16th April 2018,
Accepted 3rd June 2018

DOI: 10.1039/c8tc01779d

rsc.li/materials-c

Flexible transparent conductive films (TCFs) have attracted more and more attention because of their wide range of potential applications in optical and electronic devices. Industrial-scale manufacturing of high-performance TCFs is a challenge for a wide range of applications. Here, TCFs based on polycarbonate (PC) film successively coated with multi-walled carbon nanotubes (MWNTs) and single-walled carbon nanotubes (SWNTs) are continuously fabricated by a combined spraying and roll-to-roll (R2R) technique. Moreover, such a continuous and scalable method is programmable and fully automated. The synergism between the successively sprayed MWNTs and SWNTs significantly enhances the conductivity and electrical homogeneity of the TCFs. Furthermore, such a film (*i.e.*, PM_1S_1) still retains its high transmittance (82% at 550 nm), which is only decreased by 6% compared with the PC film. More importantly, no obvious decrease in the conductivity of the TCFs was detected after 1000 cycles of repeated bending, indicating their excellent mechanical flexibility. In addition, due to the synergistic effect, the adhesion and good environmental resistance have been significantly improved. With these advantages, the as-fabricated TCFs show great potential for application in flexible smart windows with switchable thermochromic properties. The proposed technique in this study is an effective approach for fabricating large-scale carbon nanotube/polymer based TCFs, which are promising for a wide variety of practical applications.

1. Introduction

The development and commercialization of transparent conductive films (TCFs) have drawn extensive attention recently.[1] The ideal TCFs exhibit a very low sheet resistance and high light transmission across the UV-vis-NIR spectrum.[2] TCFs are widely used as electrodes in electro-optic devices, including solar cells,[3–7] photovoltaics,[8–10] touch screen panels,[11,12] organic light-emitting diodes,[13] and transparent heaters.[14,15] The dominant TCFs used today are generally fabricated based on flexible substrates coated by indium-doped tin oxide (ITO). However, apart from the high cost and scarcity of indium sources, ITO suffers from its ceramic nature (*i.e.*, mechanical brittleness) as well, hindering its further application in flexible electronics.[16,17] To overcome these deficiencies, various alternative nanomaterials, including metal nanowires (NWs),[18,19] poly(3,4-ethylene dioxylene thiophene):poly(styrene sulfonic acid),[3] carbon nanotubes (CNTs),[8,20,21] and graphene,[11,22,23] have been emerging as candidates for TCF fabrication. Among them, CNTs have attracted great interest due to their nanoscale diameter, high aspect ratio, high conductivity and mechanical flexibility.[24,25]

With the boom of flexible electronics, mechanical flexibility has become another important measure to evaluate the performance of TCFs. The effective combination of CNTs and flexible plastic is one of the best ways to prepare flexible TCFs. Two important approaches have been developed to prepare CNT–polymer TCFs. One is the dry method, that is, films are drawn directly from CNT arrays, followed by a transfer procedure to fabricate CNT films on flexible polymer substrates,[12,26,27] another one (*i.e.*, the wet method) is dispersing CNTs in an organic solvent and then fabricating films from the solution.[1,28] Compared with the dry method, the wet method is well-known as a low-cost transfer-free route for the mass production of large-area TCFs. Many kinds of CNT–polymer TCFs have been

[a] College of Materials Science and Engineering, The Key Laboratory of Material Processing and Mold of Ministry of Education, Zhengzhou University, China. E-mail: gqzheng@zzu.edu.cn, ctliu@zzu.edu.cn
[b] Integrated Composites Laboratory (ICL), Department of Chemical & Biomolecular Engineering, University of Tennessee, Knoxville, TN 37996, USA. E-mail: zguo10@utk.edu
[c] College of Materials Science and Engineering, Shandong University of Science and Technology, Qingdao 266590, China
[d] School of Material Science and Engineering, Jiangsu University of Science and Technology, Zhenjiang, Jiangsu, 212003, China
[e] State Key Laboratory of Marine Resource Utilization in South China Sea, Hainan University, Haikou 570228, P. R. China

† Electronic supplementary information (ESI) available. See DOI: 10.1039/c8tc01779d

fabricated from solutions by various methods, including vacuum filtration,[13,29,30] spin-coating,[3] rod-coating,[31,32] spray-coating,[8,33,34] and dip-coating.[5,35] However, the continuous large-scale preparation of uniform CNT–polymer TCFs with superior optoelectronic properties and excellent mechanical flexibility is still a big challenge.[11,36] This can be ascribed to the following crucial issues: (a) inhomogeneous dispersion of high-quality CNTs in solvent; (b) the lack of a continuous large-scale fabrication method for CNT–polymer TCFs; (c) the complex and costly fabrication process. Therefore, the development of an efficient, cost-effective and scalable method to construct highly conductive CNT networks on a flexible substrate is of crucial importance.

To fabricate flexible CNT–polymer TCFs, most researchers pay more attention to the polyethylene terephthalate (PET) substrate. Polycarbonate (PC), which is usually used in the aeronautic and automotive fields, has better transparency, thermal stability and resistance and may show more advantages in the field of TCFs.[37] At present, TCFs based on PC films have rarely been developed, while most of them are limited in stability and scalable production.[38,39] For example, Hecht *et al.* reported a PC/CNT film with good conductivity, while the adhesion of CNTs on the substrate was poor.

In this paper, a roll-to-roll (R2R) spraying method was developed to continuously fabricate flexible, large-scale and transparent CNT–polymer TCFs. By combining the R2R process with simultaneous spraying, a large area PC/MWNT/SWNT film was continuously fabricated. The whole fabrication process was carried out using an automatic program control system without involving any chemical reaction. The as-prepared TCFs showed remarkable environmental resistance, strong adhesion to the substrate and balanced transparent, flexible and electrical conductive properties. The TCFs were assembled into a smart window and tested for switchable thermochromic applications. This study provides a facile, effective and low-cost way to produce CNT–polymer TCFs, which is also an important step to realize industrial-scale applications of CNTs in the fabrication of TCFs.

2. Experimental

2.1 Materials

Multi-walled carbon nanotubes (MWNTs) and single-walled carbon nanotubes (SWNTs), produced by a floating CVD method, were purchased from Chengdu Organic Chemicals Co., Ltd, China. They were dried at 80 °C under vacuum for 10 h before usage. Lexan 8010 polycarbonate (PC) film with a thickness of 125 μm (density: 1.2 g cm^{-3}) was purchased from General Electric Co. In view of these materials, CNTs were used as conductive fillers and PC as the transparent flexible substrate. Sodium dodecyl sulfate (SDS, chemically pure) was purchased from Sinopharm Chemical Reagent Co., Ltd. Acetone was purchased from Luoyang Wu Hua Chemical Reagent Co. Ltd, China. Deionized water was obtained from Nabaichuan water treatment equipment Co., Ltd. Polyurethane (PU) was purchased from Changzhou Sanhekou Polyurethane Factory. Thermochromic inks with a color transition temperature of 35 °C were purchased from Shenzhen Qianbian Pigment Co., Ltd.

2.2 Dispersion of CNTs

Pure MWNT powders (0.01 wt%) were dispersed in acetone without surfactants. This mixture was placed in an ice water bath and sonicated using an ultrasonic horn-type sonicator for 45 min at 315 W (Scientz-IID, Ningbo Scientz Biotechnology Co., China). Typically, SWNTs (0.02 wt%) and SDS (0.1 wt%) were dispersed in deionized water by ultrasonication in an ice water bath for 60 min at 315 W. Both MWNT and SWNT dispersions were centrifuged at 2000 rpm for 10 min in a high-speed desktop centrifuge (TG16-WS, Hunan Instrument Laboratory Instrument Development Co., Ltd) to remove aggregates and other impurities. The final dispersions used for further experiments were obtained by decanting the top 90% of the supernatant.

2.3 Fabrication of PC/CNT films using the R2R spraying technique

The PC/MWNT/SWNT films were continuously fabricated at room temperature using a home-made R2R spraying technique. Fig. 1a shows the schematic of the R2R spraying technique. It was mainly composed of five components: an unwinder, a substrate heating zone, a spraying system, a 2D traverse system, and a rewinder. The spraying system consists of a solution dispersion system, a compressor to provide spray droplet carrier air flow, an atomizing nozzle, and a hot plate to control the substrate temperature (Fig. S1, ESI†). The rewinder was equipped with a torque motor to keep appropriate tension of the PC film. Furthermore, the rolling speed of the PC film (herein, 90 mm min^{-1}) could be precisely controlled by the motor speed of the winder and rewind rollers. In addition, a 2D traverse system, controlled by a Numerical Control (NC) sliding table, can drive the atomizing nozzle to move at a preset speed (herein, 4000 mm min^{-1}), perpendicular to the motion direction of the PC film (Movie S1, ESI†).

CNTs were uniformly coated on the PC film through a spraying system. A syringe pump regulated the delivery of the CNT suspensions from the dispersion container into the spray nozzle. A pressure regulating valve controlled the carrier air pressure before entering into the nozzle (herein, 0.3 MPa). The distance from the atomizing nozzle to the substrate was kept constant at 50 mm, and the discharge rate of the spray precursor solution was set at 40 mL min^{-1}. Under static conditions, the atomizing nozzle was able to spray an atomizing region with a diameter of around 30 mm (seen in the inset in Fig. 1a). MWNT and SWNT dispersions were successively sprayed on the PC film and the substrate temperature was maintained at 70 °C for rapid drying of the solvent.

In a typical process, sprayed with MWNTs, the PC/MWNT film was collected and reversed for the spraying of SWNTs after a new SWNT solution was added in the nozzle. Multiple layers of CNTs were formed by increasing the number of returning cycles. For the sake of brevity, PC/MWNT/SWNT films are denoted as PM_xS_y. Herein, x and y respectively represent the number of R2R spraying cycles for MWNT and SWNT dispersions. For example, PM_1S_2 represents the PC/MWNT/SWNT

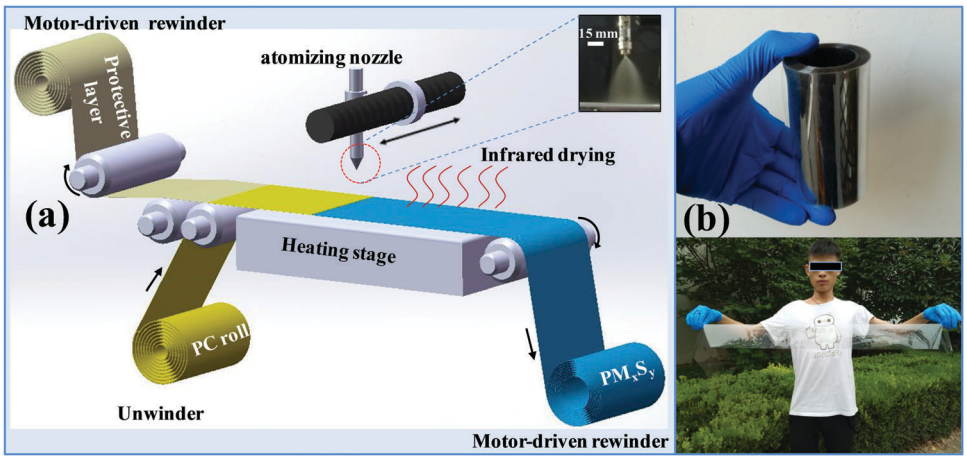

Fig. 1 Schematic diagram of the fabrication process: a R2R spraying method for continuous production (a). Inset image in (a) is the photograph of spray atomization. Photograph of a roll of PM_1S_1 (top), and that of unfolded PM_1S_1 (bottom) (b).

film that was prepared upon 1 cycle for MWNT dispersion spraying and 2 cycles of SWNT dispersion spraying.

2.4 Characterization

The sheet resistance of the PC/CNT films was measured by a four-point probe system (RTS-8, 4 PROBES TECH Co., Ltd, China) and the final value was averaged from 100 values at different positions on a sample (50 mm × 50 mm). To evaluate the uniformity of the film (such as PM_1S_1), 2000 points over a 100 mm × 100 mm film were selected (in a 2D array with a 5 mm × 5 mm lattice) (see the inset in Fig. 2d) and measured using the four-probe method (the spacing of the probes was 1 ± 0.01 mm). The current–voltage (I–V) measurement was carried out using an RST 5000-type electrochemical workstation (Zhengzhou Shiruisi Instrument Technology Co., Ltd, China) at a scanning rate of 0.05 V s^{-1} beginning at −1 V and sweeping down to 1 V. To ensure accuracy, at least 5 specimens were tested for each condition.

Transmittance was measured in the wavelength range from 400 to 1100 nm using a dual beam, ultraviolet, visible light and near infrared spectrophotometer (Agilent Cary 5000 UV-Vis-NIR Spectrophotometer) on a transparent quartz substrate.

Scanning electronic microscopy (Zeiss MERLIN Compact) was employed to investigate the distribution of CNTs on the

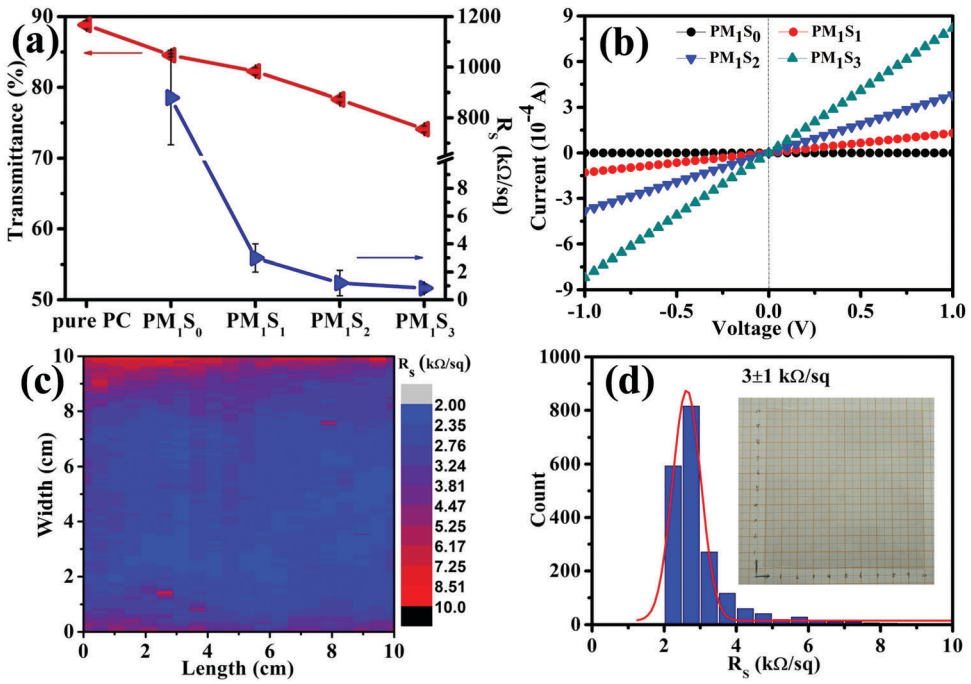

Fig. 2 Sheet resistance and transmittance at 550 nm as a function of the number of R2R spraying cycles (a). I–V curves (b). Distribution of the surface resistivity of PM_1S_1 with a size of 10 × 10 cm^2 (c). Distribution of the sheet resistance tested at 2000 points (d). Inset image in (d) is the photographs of the test sample (the background is linear coordinate paper).

surface of PC/CNT films (such as PM_1S_0 and PM_1S_1). In order to investigate the interface interaction between CNTs and the PC film, the cross-sectional morphologies of the PC/CNT films (such as PM_3S_0 and PM_1S_1) were observed. Before SEM observation, the PC/CNT films were quickly cut off by a sharp blade. All scanning surfaces were then coated with a thin layer of platinum for better SEM observation. The Fourier transform infrared (FTIR) spectra of the films were recorded using a Nicolet iS50 spectrometer in attenuated total reflection (ATR) mode.

X-ray diffraction (XRD) measurements were carried out using a Rigaku Ultima IV X-ray diffractometer, equipped with a Cu tube and a scintillation detector beam. XRD scans were recorded from 5° to 80° 2θ with a 0.02° step-width and 60 s counting time for each step.

Raman spectroscopy was used to investigate the interaction between CNTs and the polymer matrix using a Horbia Labram-010 (JobinYvon, France) with 632 nm laser excitation at 1 cm^{-1} resolution in the range from 1200 to 3400 cm^{-1}.

Differential scanning calorimetry (DSC) analysis was carried out on a DSC/MDSC2920 (TA Instruments Co., USA). Approximately 4 mg of the sample was encapsulated in an aluminum pan and heated from 40 to 300 °C at a heating rate of 10 °C min^{-1}. All the tests were performed in a nitrogen atmosphere at a flow rate of 20 mL min^{-1}.

To analyze the thermal stability and weight fraction of CNTs in the PC/CNT films, thermogravimetric analysis was performed under a nitrogen atmosphere on a Q5000IR TGA/TA (TA Instruments Co., USA). A sample of about 8 mg was heated from ambient temperature to 800 °C at a constant heating rate of 10 °C min^{-1} in a nitrogen atmosphere. The nitrogen flow rate was 25 mL min^{-1}. Five samples were tested to obtain an average value of the residue percentage.

The flexibility of the PC/CNT films (such as PM_1S_1) was evaluated upon repeating outer/inner bending. A bending durability test was carried out by measuring the resistance between two electrodes. Before the test, PM_1S_1 was first cut into rectangular shapes (50 mm × 10 mm) and both ends of the rectangle were coated with conductive silver paste to eliminate contact resistance. The mechanical properties of PM_1S_1 were investigated using a specially designed inner/outer bending system. The outer bending will induce tensile stress on the CNT layer, whereas the inner bending will induce compressive stress on the reverse side. In addition, dynamic fatigue bending tests were carried out using a home-made cyclic bending test machine, operated at a crosshead rate of 10 mm min^{-1} for 1000 cycles. The resistance of PM_1S_1 was measured during the cyclic bending process.

2.5 Switchable thermochromic applications

The pure PC film was cleaned with ethanol and dried with pressurized nitrogen before use. A sandwiched PM_1S_1/PU/PC composite film was first prepared as follows: the middle layer of the PU film with 0.2 mm thickness was hot pressed on a PC film (100 mm × 100 mm) using a compression molding machine. After that, PM_1S_1 was laid directly on the PU film.

A sandwiched PM_1S_1/thermochromic ink/PC composite film was also prepared. The thermochromic ink was coated on the PC film by spin-coating at a speed of 6000 rpm for 5 min, forming an approximately 75 μm thick layer. After that, the composite film was laid directly on PM_1S_1.

3. Results and discussion

3.1 Optoelectronic properties

Fig. 1a illustrates the schematic of the home-made R2R spraying method, which can realize continuous fabrication at room temperature. Fig. 1b (top) shows the photograph of the obtained rolled-up PM_1S_1 (width of 100 mm, length of 3000 mm). The unfolded film shows better transmittance and flexibility (Fig. 1b, bottom).

To exactly study the optoelectronic properties, the transmittances and sheet resistances of pure PC and the PC/CNT films with different R2R spraying cycles of MWNTs and SWNTs are investigated. The optical and electrical properties of the fabricated PC/MWNT films (*i.e.*, PM_xS_0) that were only sprayed with MWNTs (Fig. S2, ESI†) were first investigated. After five R2R spraying cycles, although the resistance can be decreased to 19.3 kΩ sq^{-1}, the transmittance is as low as 65.7%. In other words, both sheet resistance and transmittance are not desirable. It is well known that SWNTs have a higher conductivity compared to MWNTs when the same amount of CNTs is used. Fig. S3 (ESI†) shows a typical photograph of the PC/SWNT films (*i.e.*, PM_0S_1) that were only sprayed with SWNTs and the corresponding SEM images. The SWNT coating observed was non-uniform in both the micro- and macro-scale. Therefore, only spraying SWNTs is not the ideal choice for the preparation of PC/CNT films. To simultaneously improve the transmittance, conductivity and other properties, SWNTs and MWNTs are used jointly in the following section. Fig. 2a shows the transmittances and sheet resistances of pure PC and the as-fabricated PC/MWNT/SWNT films (PM_1S_y) with different R2R spraying cycles of SWNTs. As shown in Fig. 2a, the sheet resistance of PM_1S_y strongly depends on the spraying cycles of the SWNT dispersion. Particularly, the sheet resistance of the TCFs (*i.e.*, PM_1S_1) dramatically decreases even upon 1 spraying cycle of the SWNT dispersion. However, with further increasing the spraying cycle, the sheet resistance cannot be significantly reduced. This indicates that the ideal conductive network has been formed after only 1 spraying cycle of the SWNT dispersion, and further spraying will not make any further remarkable contribution to the improved conductivity. Fig. S4 (ESI†) shows the transmittance spectra of pure PC and PM_1S_y. It is well known that the transmittance of TCFs at 550 nm is important for opto-electronic applications due to it being the most sensitive wavelength of the human eye.[40] Thus, the transmittance at 550 nm was adopted as the major study object, as shown in Fig. 2a. Particularly, the transmittance of PM_1S_y generally decreases with increasing the R2R spraying cycle of the SWNT dispersion. However, PM_1S_1 still retains a high transmittance of 82%, which only decreases by 6% compared with the pure PC film. This should be ascribed to a uniform distribution and low content of CNTs.[41] The *I–V* curves of PM_1S_y shown in

Fig. 2b exhibit the typical Ohmic behavior, indicating the stable electrical properties. Considering the balanced transmittance and conductivity, PM_1S_1 will be employed for further study unless specifically stated.

The uniformity is another crucial factor for the large-scale production of TCFs and practical applications.[32] Fig. 2c illustrates the sheet resistance distribution of PM_1S_1. The surface resistivity reveals a mean value of 3 kΩ sq^{-1} and a standard deviation of 1 kΩ sq^{-1}, indicating a high electrical homogeneity. A statistical analysis of the sheet resistance values, presented in Fig. 2d, clearly shows that most dominant sheet resistance values fall in the range of 2–4 kΩ sq^{-1}. This suggests its good resistance uniformity, which will be necessary for further functional applications. The homogeneity of conductivity should be ascribed to the optimized spraying conditions of MWNTs and SWNTs.

3.2 Morphology

To better understand the transmittance and electrical conductivity of the TCFs, the surface morphologies of PM_1S_0 and PM_1S_1 were observed by SEM. Fig. 3a and a′ show the typical surface morphology of PM_1S_0. Generally, PM_1S_0 shows a rough surface coated with smaller aggregates of MWNTs. Although the ends of MWNTs are adhered to the surface of the PC film, an effective conductive network cannot be formed because of the sparse snake-like MWNTs (Fig. 3a′). Furthermore, from the cross-sectional morphology shown in Fig. 3b and b′, it is clear that one end of the MWNTs has entered into the interior of the PC film, while the other end suspends over the PC surface. The main reason for this is that the sprayed acetone dissolves the PC surface and allows one end of the MWNTs to easily enter the PC surface. Although the embedded end of the MWNTs may enhance the interface interaction between MWNTs and the PC film, the overall adhesion is poor, which will be proved in the following adhesion experiment. After 1 spraying cycle of SWNTs, as shown in Fig. 4a, the surface of the film (PM_1S_1) becomes rougher. It is worth noting that the isolated MWNTs and their smaller aggregates are well connected by longer SWNTs, building a spider web (Fig. 4a′). Interestingly, the suspended MWNTs are coated by SWNTs with a larger aspect ratio and are tightly adhered on the film surface (Fig. 4b and b′). Moreover, as shown in Fig. 4c and c′, almost all CNTs are tightly adhered to the PC surface and some even immersed into the interior of the PC substrate (shown by arrows in Fig. 4c′). In short, the successive spraying of MWNTs and SWNTs has a synergistic effect on promoting the adhesion of CNTs and building a good CNT network.

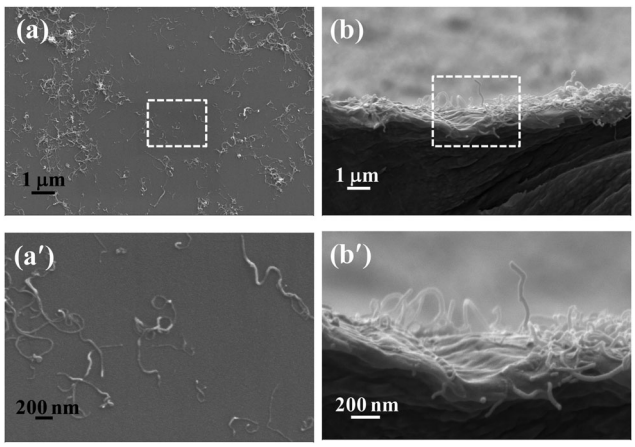

Fig. 3 Surface (a and a′) morphology of PM_1S_0 and cross-sectional (b and b′) morphology of PM_3S_0 at different magnifications.

3.3 Fourier transform infrared spectroscopy and X-ray diffraction analysis

Fig. 5a shows the FTIR spectra of MWNTs, SWNTs, pure PC and PM_1S_1. For MWNTs and SWNTs, three bands at 3425, 2924, and 1640 cm^{-1} and those in the range of 1300–950 cm^{-1} are the typical signals of the CNT structure.[42] For pure PC, the bands at 2873, 2931, and 2967 cm^{-1} are due to the C–H bond stretching. Another band at 1218 cm^{-1} is ascribed to the C–O bending vibration. For C═O, the band at 1768 cm^{-1} is observed.[42] However, several bands for pure PC are found to have shifted after the spraying of MWNTs and SWNTs. For example, the band

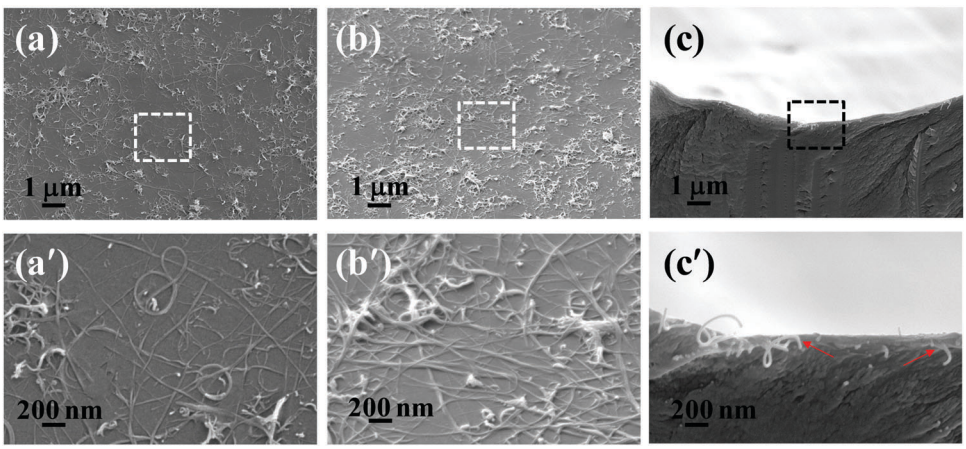

Fig. 4 Surface (a, a′, and b, b′) and cross-sectional (c and c′) morphology of PM_1S_1 at different magnifications. SEM images (b and b′) taken from a perspective angle (45° from the normal direction).

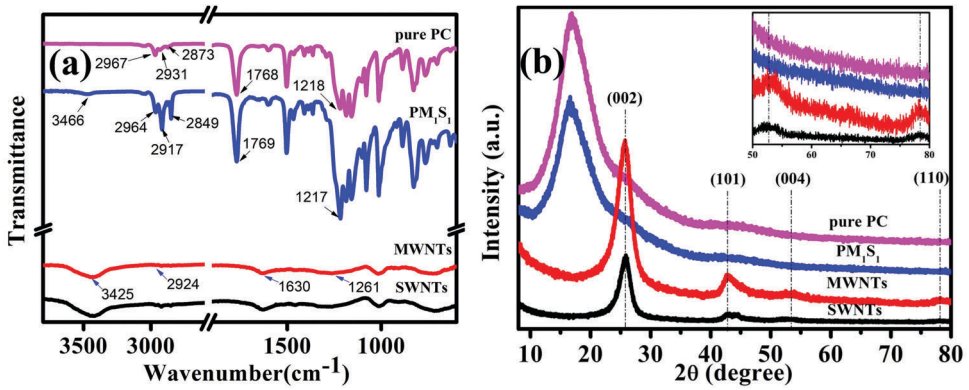

Fig. 5 FTIR spectra (a) and XRD spectra (b) of SWNTs, MWNTs, pure PC and PM_1S_1.

at 2931 cm^{-1} has shifted to 2917 cm^{-1} and that at 2873 cm^{-1} has shifted to 2849 cm^{-1}. These changes suggest chemical interactions between the PC macromolecular chain and CNTs.[43,44]

The microstructure of the TCFs is of further interest and it was studied by XRD and the results are shown in Fig. 5b. It can be clearly seen that there are four dominant peaks at 2θ = 25.85°, 42.85°, 53.56° and 78.27°, which correspond to the hexagonal graphite planes (002), (101), (004) and (110) of CNTs, respectively.[45] Moreover, pure PC shows a broad peak (halo) at around 2θ = ~16.73°, indicating its amorphous nature.[46] Compared with pure PC, the characteristic peak of PC in PM_1S_1 shows no obvious difference in position. However, its intensity is attenuated after the decoration of CNTs. This phenomenon should be ascribed to the interfacial interaction between PC and CNTs. The disappearance of these peaks could be ascribed to the homogeneous dispersion of CNTs on the PC film, which can be confirmed by our previous study.[47] On the other hand, the mass of CNTs in this composite film is very low relative to PC, and their characteristic peaks might be shielded by the characteristic peaks of PC.

3.4 Raman spectroscopy and differential scanning calorimetry analysis

Raman spectroscopy was further performed to analyze the interface interaction between the CNTs and the PC film. The main characteristic peaks are shown in Fig. 6a. For MWNTs and SWNTs, three typical peaks at 1323, 1591, and 2639 cm^{-1} respectively corresponding to the D, G, and 2D bands are the signals of the CNT structure.[48] As is well known, the D band is related to the defects induced by disorder, whereas the G and 2D bands correspond to the in-plane vibration of the C–C bond.[49,50] For pure PC, three typical peaks at 1232, 1603, and 1773 cm^{-1} are the characteristic vibration bands of PC.[51] In the spectrum of PM_1S_1, the characteristic bands of CNTs are easily identified. Compared with the spectra of SWNTs and MWNTs, it is worth noting that several characteristic bands of CNTs in PM_1S_1 have been up-shifted. For example, the D band peak is up-shifted from 1324 to 1395 cm^{-1} and the G band increased from 1591 to 1601 cm^{-1}. Moreover, other PC characteristic bands are attenuated or even disappear after the spraying of MWNTs and SWNTs. The above observations suggest the existence of a strong interface interaction between pure PC and CNTs.[52]

DSC experiments were also carried out to investigate the effects of the interaction on the thermal properties of the film, such as the glass transition temperature. Fig. 6b shows that the glass transition temperature (T_g) of pure PC is about 149.94 °C. However, after the spraying of MWNTs and SWNTs, the T_g of PM_1S_1 increased to 151.08 °C. From this viewpoint, an interface interaction occurs between PC and CNTs.[53]

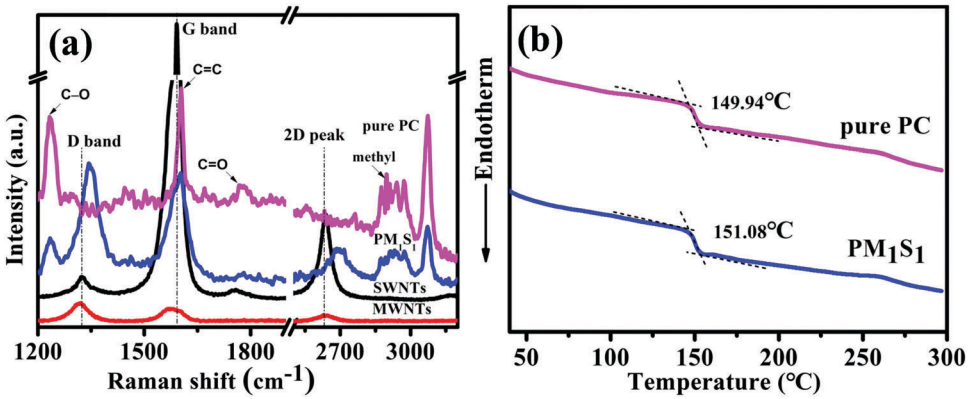

Fig. 6 Raman spectra of SWNTs, MWNTs, pure PC and PM_1S_1 (a). DSC curves of pure PC and PM_1S_1 (b).

3.5 Thermal stability

TGA was carried out to evaluate the thermal stability and the CNT content of the TCFs. Fig. 7 shows the TGA curve and the corresponding differential thermogravimetric (DTG) curve. As shown in Fig. 7a, the onset degradation temperature of PM_1S_1 shifts towards higher temperature compared with pure PC and PM_1S_0. Moreover, compared with pure PC and PM_1S_0, the temperature of maximum degradation rate (T_{max}) of PM_1S_1 increases from 495 °C to around 508 °C, suggesting that the successive spraying of MWNTs and SWNTs can improve the thermal stability (see Fig. 7b). The CNT content of TCFs can be obtained from TGA. After the successive spraying of MWNTs and SWNTs, the total CNT content in PM_1S_1 was 0.77 wt%.[54,55]

3.6 Adhesive properties

Strong adhesion is of significant concern for TCFs because poor adhesion of CNTs to the substrate may hinder their practical applications.[23] Fig. 8a shows the resistance change of PM_1S_1 and PM_3S_0 upon repeated Scotch tape peeling. Note, the conductivity of PM_3S_0 can be thoroughly damaged even after 1 peeling cycle. However, the conductivity of PM_1S_1 does not degrade upon repeated Scotch tape peeling, even up to 100 cycles. Obviously, pure MWNTs have the poorest adhesion to PC while the combination of MWNTs and SWNTs can significantly enhance the adhesion. For PM_3S_0, as shown in Fig. 3b′, the segments of MWNTs are suspended over the surface of PC and are tightly adhered to the Scotch tape.

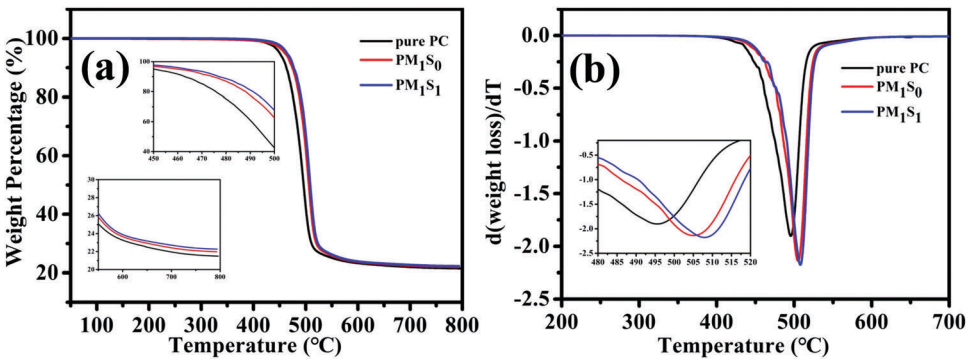

Fig. 7 TGA curves (a) and DTG curves (b) of pure PC, PM_1S_0 and PM_1S_1.

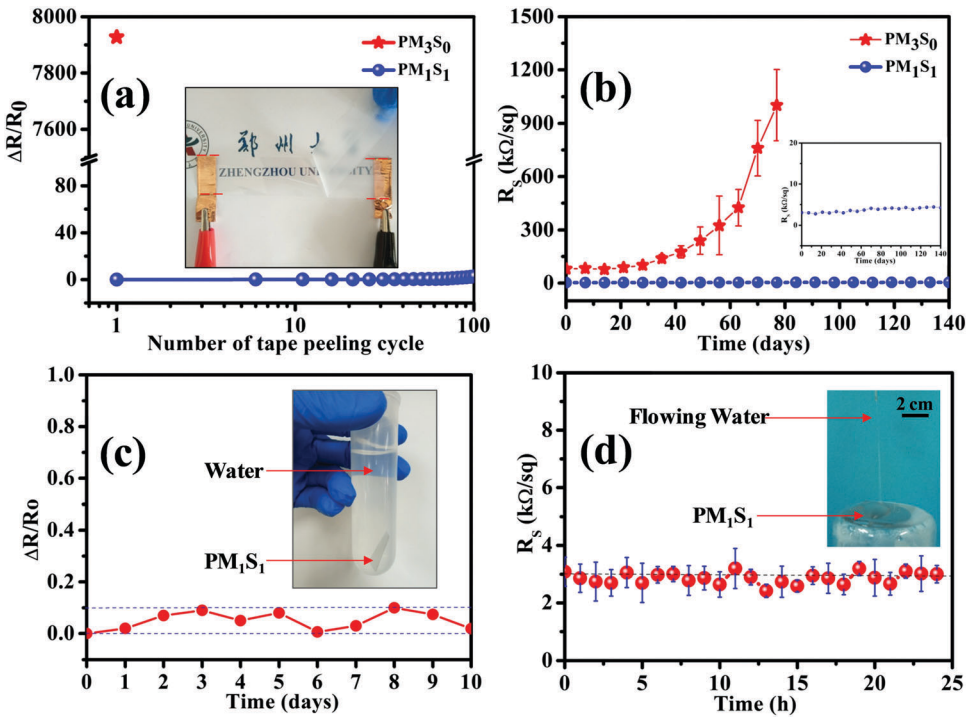

Fig. 8 The durability of PC/CNTs films. Resistance variation as a function of cycle number upon peeling by 3M Scotch tape (a). Resistance variation of TCFs exposed to air at room temperature for 140 days (b). Resistance variation of PM_1S_1 soaked in water for 10 days (c). Resistance variation of PM_1S_1 upon the impact of flowing water (d).

Therefore, it is reasonable that they can be easily wiped off from the substrate. For PM_1S_1, after solely spraying MWNTs, the surface of PC becomes rough, which is equivalent to the micro-nano treatment on the surface. This micro-nano structure is beneficial for the entrapment of SWNTs on the surface of PC, which results in strong adhesion even in the absence of a binder.[33,56] On the other hand, due to van der Waals interactions between MWNTs, SWNTs and PC,[57] the embedded MWNTs act as a bridge connecting SWNTs and PC, resulting in SWNTs anchoring onto the film tightly (see Fig. 4a and a′).

Excellent environment resistance is another important issue for the application of TCFs.[23] Fig. 8b shows the resistance change of PM_1S_1 and PM_3S_0 exposed to the atmosphere at room temperature for 140 days. Clearly, the resistance of PM_3S_0 increases significantly after 20 days of exposure to the atmosphere. However, the resistance of PM_1S_1 does not change even after 140 days. In addition, the conductivity of PM_1S_1 did not change significantly even though it was immersed in water for 10 days (Fig. 8c). More interestingly, PM_1S_1 can bear attack by flowing water, which lasts as long as 24 hours (Fig. 8d). That is, with increasing the time of water impact, the sheet resistance does not change significantly. The above results firmly demonstrate that PM_1S_1 shows better environmental stability compared to PM_3S_0.

3.7 Flexible properties

The mechanical properties, particularly the fold ability, are another critical factor for flexible device applications.[11] To the understand bending properties, they were characterized with $\Delta l/l_0 = (l_0 - l)/l_0$ as a criterion, where l_0 is the length of the film and l is the distance between two ends of the bending state (see the inset of Fig. 9b). The mechanical flexibility of PM_1S_1 was evaluated through inner and outer bending and cyclic fatigue tests using a home-made bending test system (see Fig. 9a). Fig. 9a illustrates the relation between $\Delta R/R_0$ and $\Delta l/l_0$. $\Delta R/R_0$ is defined as $\Delta R/R_0 = (R_t - R_0)/R_0$, where R_0 is the initial resistance and R_t is the measured resistance after bending. The sheet resistance change curves of PM_1S_1 were tested under different bending strains (for example, 10%, 20%, 40%, 60%, and 80%). As shown in Fig. 9a, regardless of the inner or outer bending, PM_1S_1 generally exhibits constant resistance not only at low bending strain but also at the bending limit of 80%. Fig. 9b shows the dynamic outer and inner bending fatigue test results of PM_1S_1 with increasing the bending cycle at a fixed bending strain of 50%. Even after 1000 bending cycles, both the outer and inner cyclic bending fatigue tests show no obvious change in the resistance (ΔR), demonstrating the superior flexibility of PM_1S_1.

In summary, the aforementioned strong adhesion, high environmental stability, superior flexibility and high thermal stability of TCFs should be ascribed to the strong interaction between CNTs and the PC film.

3.8 Applications for switchable thermochromism

The fabrication of a uniformly interconnected CNT network is crucial to achieve a homogeneous temperature distribution in CNT derived transparent heaters. The uniformity of the fabricated TCFs was tested by Joule heating followed by infrared thermal imaging.[58] Fig. 10a shows the infrared thermal image of PM_1S_1 taken using an infrared thermal imaging camera (FLIR T650sc) with a constant DC voltage of 80 V. The transparent heater shows a relatively uniform temperature distribution across a large area, which is consistent with the uniform sheet resistance distribution shown in Fig. 2c. Furthermore, under a bending strain of 50%, the transparent heater can also work well (Fig. 10b). Therefore, it can serve as an ideal choice for the fabrication of flexible electronic devices.

Smart windows have attracted increasing attention with intriguing functions, such as switchable transparency and thermochromism. The progress in this field has been promoted with the development of transparent electrode technology. However, as a common transparent electrode material, ITO may restrict the development of smart windows because of its inflexibility, high-cost, and limitation in large-area and scalable production. Therefore, it still remains a challenge to find ideal transparent electrodes for smart windows. In our work, considering its high transparency, good electrical conductivity and excellent flexibility, the as-prepared PM_1S_1 is used successfully

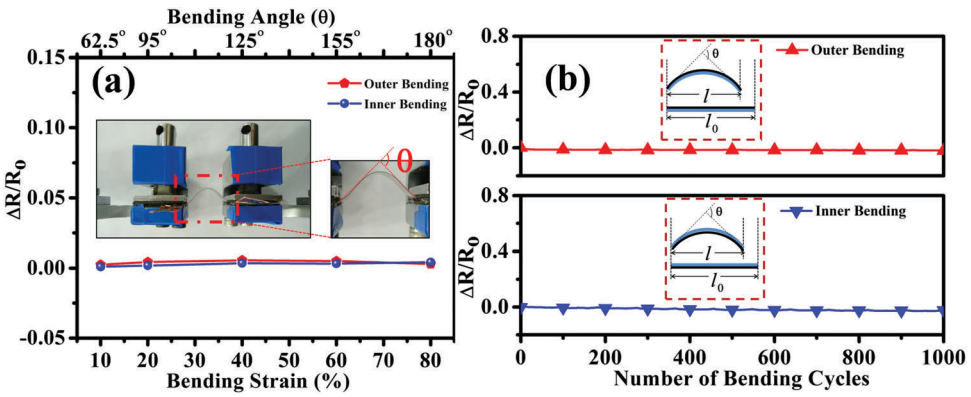

Fig. 9 (a) Outer and inner bending test results at different bending strains. The inset shows the automatic bending apparatus used in this study. (b) Cyclic outer and inner fatigue test results of PM_1S_1 at a bending strain of 50% with increasing bending cycles. Inset is a schematic diagram when the film was bent.

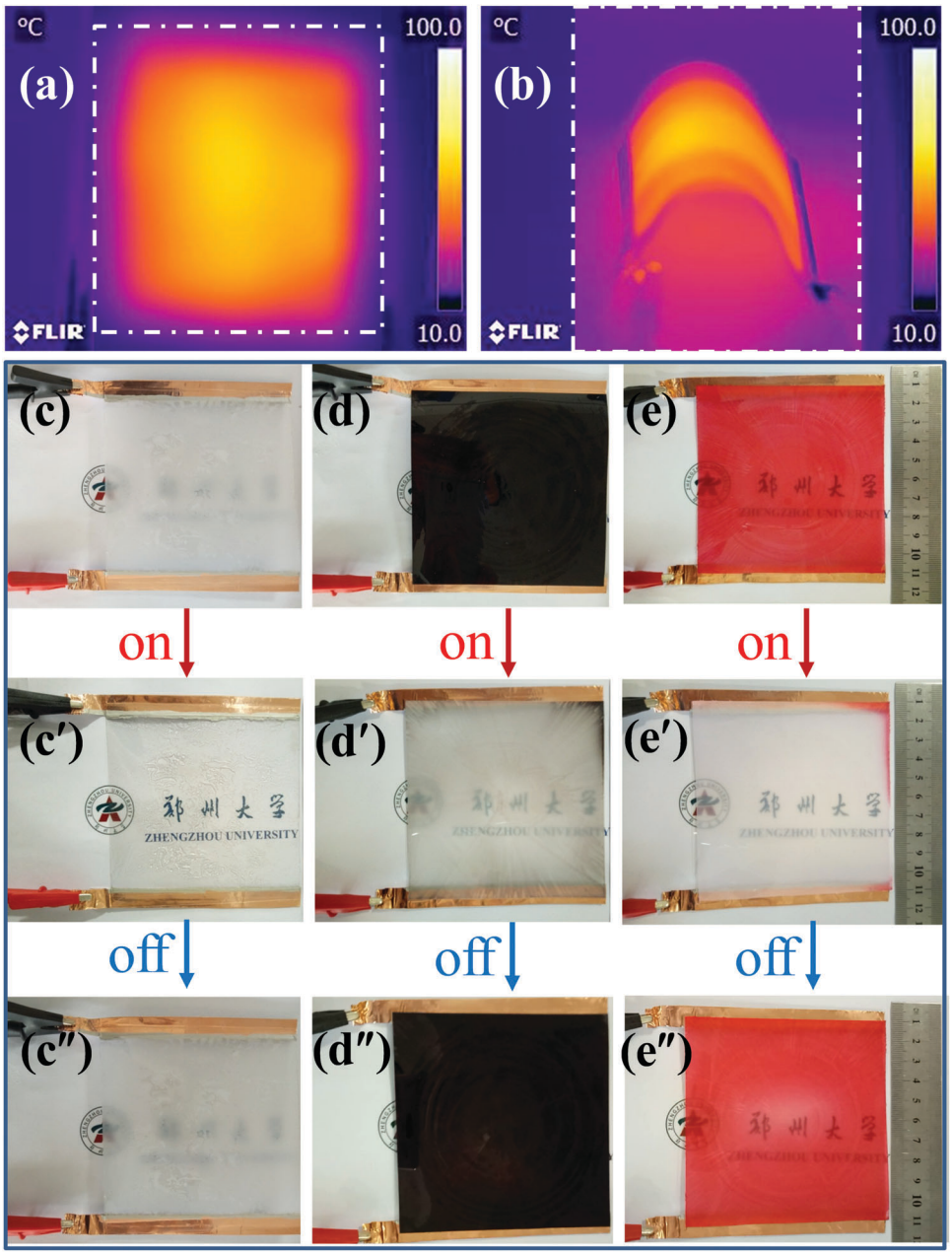

Fig. 10 Infrared thermal image of PM_1S_1 (10 × 10 cm^2) for a transparent heater (a) and that under a bending strain of 50% (b). An opaque composite film is connected to two copper electrodes (c), switches from opaque to transparent after turning on voltage (c′), and reverses back to opaque after turning off voltage (c″). Heat-induced thermochromism (from top to bottom) is also observed in two dyed films (d–d″ and e–e″).

as an electrode for the fabrication of smart windows. Above all, its Joule heating property is further studied. Resistive Joule heating is induced by applying a constant DC voltage at both ends of the PM_1S_1 electrode. Fig. S5 (ESI†) shows the temperature–time curves of PM_1S_1 at different voltages. Clearly, when a DC voltage is applied, the temperature gradually increases and reaches a maximum that is proportional to the applied pulse voltage. Moreover, it can steadily return to the original room temperature after removing the voltage. A 10 × 10 cm^2 composite film (PC/PU/PM_1S_1) for smart windows was firstly fabricated with a typical sandwiched structure in this work (Fig. S6, ESI†). The composite film is initially opaque (Fig. 10c), while it becomes transparent after a certain voltage is applied (Fig. 10c′). Then, it turns back to an opaque state when the voltage is turned off (Fig. 10c″). The whole process can be seen in Fig. S7 in the ESI.† The opaque-to-transparent transition can be ascribed to the following fact: herein, the melting point of PU confirmed by DSC is 46.6 °C (Fig. S8, ESI†).[59] When the voltage is applied, the temperature of the composite film rapidly reaches over 70 °C (above the melting temperature of PU), thus the PU crystal will melt and the composite film transforms into a transparent state. When the voltage is turned

off, the temperature returns to room temperature (below the melting temperature of PU), resulting in the crystallization of PU with an opaque state. This opaque-to-transparent transformation can be controlled with the on–off switch of the voltage. Moreover, the reversible behavior can also be observed in two thermochromic composite films (see Fig. 10d and e). The thermochromic ink used here has different colors at low temperature and high temperature. When a certain voltage is applied, the film shown in Fig. 10d turns from black to white (Fig. 10d′), and the film shown in Fig. 10e turns from red to white (Fig. 10e′). When the voltage is off, the films return to their initial color (Fig. 10d″ and e″). The whole process can be seen in Fig. S9 and S10 (ESI†). These switchable thermochromic properties are attributed to the ohmic heating under a certain voltage. The color-changing process could be repeated due to the heating/cooling cycling stability of PM_1S_1 and the color reversibility of the thermochromic inks. It is worth noting that our fabricated TCFs have the advantages of stability and easy fabrication over those silver nanofiber-based or organic polymer-based TCFs that might be easily oxidized in air.[3,18,40] Overall, the aforementioned results demonstrate the potential capability of the fabricated TCFs in switchable thermochromism for flexible smart windows.

4. Conclusions

Large area flexible and transparent PC/MWNT/SWNT composite films were successfully fabricated by a home-made R2R spraying technique combined with successive spraying of MWNTs and SWNTs. The combination of MWNTs and SWNTs exhibited a synergistic effect to obtain good optoelectronic properties, excellent flexibility and strong adhesion to the substrate. Specifically, successive spraying of MWNTs and SWNTs enhanced the adhesion, which could protect the film from damage for further applications. Moreover, a big sheet (10×10 cm^2) multifunctional smart window with switchable transparency and thermochromic applications was successfully fabricated using the as-prepared composite film as the electrode. The opaque-to-transparent transition and color-changing of the composite films can be easily controlled by altering the voltage. The experimental results also demonstrate its good mechanical flexibility, exceeding that of the ITO-based smart windows. Moreover, the room-temperature R2R spraying procedure shows promising potential in the mass production of TCFs at low cost, which will also accelerate the actual implementation of this composite film in the fabrication of new-generation flexible smart windows and functional composites with other unique nanofillers for other applications such as energy storage/conversion,[60] environmental remediation,[61] sensing,[62] functional coating,[63] and electromagnetic interference (EMI) shielding,[64] and biomedical field.[65]

Conflicts of interest

There are no conflicts to declare.

Acknowledgements

We express our great thanks to the National Natural Science Foundation of China (11432003 and 11572290), the Major State Basic Research Projects (2012CB025904), HASTIT and the Plan for Scientific Innovation Talent of Henan Province for financial support.

References

1 Y. L. Huang, H. W. Tien, C. C. M. Ma, C. C. Teng, Y. H. Yu, S. Y. Yang, M. H. Wei and S. Y. Wu, *Appl. Surf. Sci.*, 2011, **258**, 136–142.
2 L. Yu, C. Shearer and J. Shapter, *Chem. Rev.*, 2016, **116**, 13413–13453.
3 S. Kim, J. Yim, X. Wang, D. D. C. Bradley, S. Lee and J. C. Demello, *Adv. Funct. Mater.*, 2010, **20**, 2310–2316.
4 (*a*) S. G. Hashmi, T. Moehl, J. Halme, Y. Ma, T. Saukkonen, A. Yella, F. Giordano, J. D. Decoppet, S. M. Zakeeruddin, P. Lund and M. Grätzel, *J. Mater. Chem. A*, 2014, **2**, 19609–19615; (*b*) T. Liu, K. Yu, L. Gao, H. Chen, N. Wang, L. Hao, T. Li, H. He and Z. Guo, *J. Mater. Chem. A*, 2017, **5**, 17848–17855; (*c*) H. Du, C. Zhao, J. Lin, Z. Hu, Q. Shao, J. Guo, B. Wang, D. Pan, E. K. Wujcik and Z. Guo, *Chem. Rec.*, DOI: 10.1002/tcr.201800008; (*d*) C. Wang, B. Mo, Z. He, Q. Shao, D. Pan, E. Wujick, J. Guo, X. Xie, X. Xie and Z. Guo, *J. Membr. Sci.*, 2018, **556**, 118–125; (*e*) H. Chen, T. Liu, B. Wang, Z. Liu, Y. Li, Q. Zhao, N. Wang, H. He, H. Liu and Z. Guo, *Adv. Compos. Hybrid Mater.*, 2018, **1**, 1–8.
5 Z. Yang, T. Chen, R. He, G. Guan, H. Li, L. Qiu and H. Peng, *Adv. Mater.*, 2011, **23**, 5436–5439.
6 S. Huang, Z. Yang, L. Zhang, R. He, T. Chen, Z. Cai, Y. Luo, H. Lin, H. Cao and X. Zhu, *J. Mater. Chem.*, 2012, **22**, 16833–16838.
7 (*a*) J. Han, S. Yuan, L. Liu, X. Qiu, H. Gong, X. Yang, C. Li, Y. Hao and B. Cao, *J. Mater. Chem. A*, 2015, **3**, 5375–5384; (*b*) Q. Hou, J. Ren, H. Chen, P. Yang, Q. Shao, M. Zhao, X. Zhao, H. He, N. Wang, Q. Luo and Z. Guo, *ChemElectroChem*, 2008, **5**, 726–731; (*c*) Q. Luo, H. Ma, Q. Hou, Y. Li, J. Ren, X. Dai, Z. Yao, Yu. Zhou, L. Xiang, H. Du, H. He, N. Wang, K. Jiang, H. Lin, H. Zhang and Z. Guo, *Adv. Funct. Mater.*, 2018, **28**, 1706777; (*d*) Q. Luo, H. Chen, Y. Lin, H. Du, Q. Hou, F. Hao, N. Wang, Z. Guo and J. Huang, *Adv. Funct. Mater.*, 2017, **27**, 1702090; (*e*) W. Hu, T. Liu, X. Yin, H. Liu, X. Zhao, S. Luo, Y. Guo, Z. Yao, J. Wang, N. Wang, H. Lin and Z. Guo, *J. Mater. Chem. A*, 2017, **5**, 1434–1441; (*f*) Q. Jiang, L. Wang, C. Yan, C. Liu, Z. Guo and N. Wang, *Eng. Sci.*, 2018, **1**, 64–68, DOI: 10.30919/es.180329.
8 R. C. Tenent, T. M. Barnes, J. D. Bergeson, A. J. Ferguson, B. To, L. M. Gedvilas, M. J. Heben and J. L. Blackburn, *Adv. Mater.*, 2010, **21**, 3210–3216.
9 Z. Yang, L. Li, Y. Luo, R. He, L. Qiu, H. Lin and H. Peng, *J. Mater. Chem. A*, 2013, **1**, 954–958.
10 Z. Zhang, L. Wang, Y. Li, X. Li, G. Guan, Y. Zhang and H. Peng, *J. Mater. Chem. C*, 2016, **4**, 1144–1148.
11 J. Wang, M. Liang, Y. Fang, T. Qiu, J. Zhang and L. Zhi, *Adv. Mater.*, 2012, **24**, 2874.

12 C. Feng, K. Liu, J. S. Wu, L. Liu, J. S. Cheng, Y. Zhang, Y. Sun, Q. Li, S. Fan and K. Jiang, *Adv. Funct. Mater.*, 2010, **20**, 885–891.
13 D. Zhang, K. Ryu, X. Liu, E. Polikarpov, J. Ly, M. E. Tompson and C. Zhou, *Nano Lett.*, 2006, **6**, 1880–1886.
14 (*a*) L. He and S. C. Tjong, *J. Mater. Chem. C*, 2016, **4**, 7043–7051; (*b*) Z. Hu, Q. Shao, Y. Huang, L. Yu, D. Zhang, X. Xu, J. Lin, H. Liu and Z. Guo, *Nanotechnology*, 2018, **29**, 185602.
15 R. Gupta, K. D. M. Rao, S. Kiruthika and G. U. Kulkarni, *ACS Appl. Mater. Interfaces*, 2016, **8**, 12559–12575.
16 K. Ellmer, *Nat. Photonics*, 2012, **6**, 809–817.
17 A. Kumar and C. Zhou, *ACS Nano*, 2010, **4**, 11–14.
18 A. R. Rathmell and B. J. Wiley, *Adv. Mater.*, 2011, **23**, 4798–4803.
19 Y. Liu, Q. Chang and L. Huang, *J. Mater. Chem. C*, 2013, **1**, 2970–2974.
20 Z. Wu, Z. Chen, X. Du, J. M. Logan, J. Sippel, M. Nikolou, K. Kamaras, J. R. Reynolds, D. B. Tanner and A. F. Hebard, *Science*, 2004, **305**, 1273–1276.
21 E. X. Ding, H. Jiang, Q. Zhang, Y. Tian, P. Laiho, A. Hussain, Y. Liao, N. Wei and E. I. Kauppinen, *Nanoscale*, 2017, **9**, 17601–17609.
22 J. Ning, L. Hao, M. Jin, X. Qiu, Y. Shen, J. Liang, X. Zhang, B. Wang, X. Li and L. Zhi, *Adv. Mater.*, 2017, **29**, 1605028.
23 B. Deng, P. C. Hsu, G. Chen, B. N. Chandrashekar, L. Liao, Z. Ayitimuda, J. Wu, Y. Guo, L. Lin, Y. Zhou, M. Aisijiang, Q. Xie, Y. Cui, Z. Liu and H. Peng, *Nano Lett.*, 2015, **15**, 4206–4213.
24 S. Iijima, *Nature*, 1991, **354**, 56–58.
25 R. H. Baughman, A. A. Zakhidov and W. A. d. Heer, *Science*, 2002, **297**, 787–792.
26 Q. Zhang, N. Wei, P. Laiho and E. I. Kauppinen1, *Top. Curr. Chem.*, 2017, **375**, 90.
27 D. M. Sun, M. Y. Timmermans, A. Kaskela, A. G. Nasibulin, S. Kishimoto, T. Mizutani, E. I. Kauppine and Y. Ohno, *Nat. Commun.*, 2013, **4**, 2302.
28 I. O'Connor, S. De, J. N. Coleman and Y. K. Gun'ko, *Carbon*, 2009, **47**, 1983–1988.
29 P. Hou, B. Yu, Y. Su, C. Shi, L. Zhang, C. Liu, S. Li, J. Du and H. Cheng, *J. Mater. Chem. A*, 2014, **2**, 1159–1164.
30 P. X. Hou, B. Yu, Y. Su, C. Shi, L. L. Zhang, C. Liu, S. Li, J. H. Du and H. M. Cheng, *J. Mater. Chem. A*, 2014, **2**, 1159–1164.
31 S. Azoz, A. L. Exarhos, A. Marquez, L. M. Gilbertson, S. Nejati, J. J. Cha, J. B. Zimmerman, J. M. Kikkawa and L. D. Pfefferle, *Langmuir*, 2015, **31**, 1155–1163.
32 B. Dan, G. C. Irvin and M. Pasquali, *ACS Nano*, 2009, **3**, 835–843.
33 M. Karakaya, J. Zhu, A. J. Raghavendra, R. Podila, S. G. P. Jr, J. P. Kaplan and A. M. Rao, *Appl. Phys. Lett.*, 2015, **105**, 263103.
34 Q. Liu, T. Fujigaya, H. M. Cheng and N. Nakashima, *J. Am. Chem. Soc.*, 2010, **132**, 16581–16586.
35 F. Mirri, A. W. Ma, T. T. Hsu, N. Behabtu, S. L. Eichmann, C. C. Young, D. E. Tsentalovich and M. Pasquali, *ACS Nano*, 2012, **6**, 9737–9744.
36 Y. Wang, X. Liu, M. Lian, G. Zheng, K. Dai, Z. Guo, C. Liu and C. Shen, *Appl. Mater. Today*, 2017, **9**, 77–81.
37 (*a*) M. R. S. Castro, N. Al-Dahoudi, P. W. Oliveira and H. K. Schmidt, *J. Nanopart. Res.*, 2009, **11**, 801–806; (*b*) F. Luo, X. Liu, C. Shao, J. Zhang, C. Shen and Z. Guo, *Mater. Des.*, 2018, **144**, 25–31; (*c*) X. Cui, G. Zhu, Y. Pan, Q. Shao, C. Zhao, M. Dong, Y. Zhang and Z. Guo, *Polymer*, 2018, **138**, 203–210; (*d*) M. Zhao, L. Meng, L. Ma, L. Ma, X. Yang, Y. Huang, J. Ryu, A. Shankar, T. Li, C. Yan and Z. Guo, *Compos. Sci. Technol.*, 2018, **154**, 28–36; (*e*) K. Zhang, G. Li, L. Feng, N. Wang, J. Guo, K. Sun, K. Yu, J. Zeng, T. Li, Z. Guo and M. Wang, *J. Mater. Chem. C*, 2017, **5**, 9359–9369.
38 D. S. Hecht, K. A. Sierros, R. S. Lee, C. Ladous, C. Niu, D. A. Banerjee and D. R. Cairns, *J. Soc. Inf. Disp.*, 2011, **19**, 157–162.
39 A. Patole and G. Lubineau, *Carbon*, 2015, **81**, 720–730.
40 S. Lin, X. Bai, H. Wang, H. Wang, J. Song, K. Huang, C. Wang, N. Wang, B. Li and M. Lei, *Adv. Mater.*, 2017, **29**, 1703238.
41 D. Mardare and G. I. Rusu, *Mater. Lett.*, 2002, **56**, 210–214.
42 R. Kumar, Kamakshi, M. Kumar and K. Awasthi, *Int. J. Hydrogen Energy*, 2016, **41**, 23057–23066.
43 H. Liu, M. Dong, W. Huang, J. Gao, K. Dai, J. Guo, G. Zheng, C. Liu, C. Shen and Z. Guo, *J. Mater. Chem. C*, 2016, **5**, 73–83.
44 Y. Wang, J. Hao, Z. Huang, G. Zheng, K. Dai, C. Liu and C. Shen, *Carbon*, 2018, **126**, 360–371.
45 (*a*) J. Al-Osaimi, N. Alhosiny, A. Badawi and S. Abdallah, *Int. J. Eng. Technol. IJET-IJENS*, 2013, **13**, 77–79; (*b*) F. Liu, Z. Xu, Z. Wang, M. Dong, J. Deng, Q. Yao, H. Zhou, Y. Ma, J. Zhang, N. Wang and Z. Guo, *J. Alloys Compd.*, 2018, **756**, 26–32; (*c*) Z. Zhao, R. Guan, J. Zhang, Z. Zhao and P. Bai, *Acta Metall. Sin.*, 2017, **30**, 66–72.
46 P. K. Sain, R. K. Goyal, A. K. Bhargava and Y. V. S. S. Prasad, *J. Phys. D: Appl. Phys.*, 2013, **46**, 1–8.
47 A. K. Barick and D. K. Tripathy, *Mat. Sci. Eng., B*, 2011, **176**, 1435–1447.
48 T. Mcnally, P. Pötschke, P. Halley, M. Murphy, D. Martin, S. E. J. Bell, G. P. Brennan, D. Bein, P. Lemoine and J. P. Quinn, *Polymer*, 2005, **46**, 8222–8232.
49 L. Valentini, J. Biagiotti, J. M. Kenny and S. Santucci, *Compos. Sci. Technol.*, 2003, **63**, 1149–1153.
50 A. M. Bittner, M. Zhu, Y. Yang, H. F. Waibel, M. Konuma, U. Starke and C. J. Weber, *J. Power Sources*, 2012, **203**, 262–273.
51 P. Liu, Z. Jin, G. Katsukis, L. W. Drahushuk, S. Shimizu, C. J. Shih, E. D. Wetzel, J. K. Taggart-Scarff, B. Qing and K. J. Van Vliet, *Science*, 2016, **353**, 364–367.
52 Y. Li, B. Zhou, G. Zheng, X. Liu, T. Li, C. Yan, C. Cheng, K. Dai, C. Liu, C. Shen and Z. Guo, *J. Mater. Chem. C*, 2018, **6**, 2258–2269.
53 L. Liu, A. H. Barber, S. Nuriel and H. D. Wagner, *Adv. Funct. Mater.*, 2005, **15**, 975–980.
54 X. Guan, G. Zheng, K. Dai, C. Liu, X. Yan, C. Shen and Z. Guo, *ACS Appl. Mater. Interfaces*, 2016, **8**, 14150–14159.
55 J. Gao, M. Hu and R. K. Y. Li, *J. Mater. Chem.*, 2012, **22**, 10867–10872.

56 Y. J. Kang, H. Chung, M. S. Kim and W. Kim, *Appl. Surf. Sci.*, 2015, **355**, 160–165.
57 L. Hu, M. Pasta, F. L. Mantia, L. Cui, S. Jeong, H. D. Deshazer, J. W. Choi, S. M. Han and Y. Cui, *Nano Lett.*, 2010, **10**, 708–714.
58 R. Gupta, K. D. Rao, K. Srivastava, A. Kumar, S. Kiruthika and G. U. Kulkarni, *ACS Appl. Mater. Interfaces*, 2014, **6**, 13688–13696.
59 F. Meng, X. Zhang, G. Xu, Z. Yong, H. Chen, M. Chen, Q. Li and Y. Zhu, *ACS Appl. Mater. Interfaces*, 2011, **3**, 658–661.
60 (*a*) W. Deng, T. Kang, H. Liu, J. Zhang, N. Wang, N. Lu, Y. Ma, A. Umar and Z. Guo, *Sci. Adv. Mater.*, 2018, **10**, 937–949; (*b*) X. Wang, X. Zeng and D. Cao, *Eng. Sci.*, 2018, **1**, 55–63, DOI: 10.30919/es.180325; (*c*) Q. Luo, H. Ma, F. Hao, Q. Hou, J. Ren, L. Wu, Z. Yao, Y. Zhou, N. Wang, K. Jiang, H. Lin and Z. Guo, *Adv. Funct. Mater.*, 2017, **27**, 1703068.
61 (*a*) Y. Ma, L. Lyu, Y. Guo, Y. Fu, Q. Shao, T. Wu, S. Guo, K. Sun, X. Guo, E. K. Wujcik and Z. Guo, *Polymer*, 2017, **128**, 12–23; (*b*) Y. Wang, P. Zhou, S. Luo, S. Guo, J. Lin, Q. Shao, X. Guo, Z. Liu, J. Shen, B. Wang and Z. Guo, *Adv. Polym. Technol.*, 2018, DOI: 10.1002/adv.21969; (*c*) Y. Wang, P. Zhou, S. Luo, X. Liao, B. Wang, Q. Shao, X. Guo and Z. Guo, *Langmuir*, 2018, DOI: 10.1021/acs.langmuir.8b00789; (*d*) S. Sun, L. Zhu, X. Liu, L. Wu, K. Dai, C. Liu, C. Shen, X. Guo, G. Zheng and Z. Guo, *ACS Sustainable Chem. Eng.*, 2018, DOI: 10.1021/acssuschemeng.8b01047; (*e*) K. Gong, Q. Hu, Y. Xiao, X. Cheng, H. Liu, N. Wang, B. Qiu and Z. Guo, *J. Mater. Chem. A*, 2018, **6**, 11119–11128.
62 H. Gu, H. Zhang, J. Lin, Q. Shao, D. P. Young, L. Sun, T. D. Shen and Z. Guo, *Polymer*, 2018, **143**, 324–330.
63 (*a*) Y. Zhang, M. Zhao, J. Zhang, Q. Shao, J. Li, H. Li, B. Lin, M. Yu, S. Chen and Z. Guo, *J. Polym. Res.*, 2018, **25**, 130; (*b*) Z. Wu, H. Cui, L. Chen, D. Jiang, L. Weng, Y. Ma, X. Li, X. Zhang, H. Liu, N. Wang, J. Zhang, Y. Ma, M. Zhang, Y. Huang and Z. Guo, *Compos. Sci. Technol.*, 2018, **164**, 195–203; (*c*) K. Sun, R. Fan, X. Zhang, Z. Zhang, Z. Shi, N. Wang, P. Xie, Z. Wang, G. Fan, H. Liu, C. Liu, T. Li, C. Yan and Z. Guo, *J. Mater. Chem. C*, 2018, **6**, 2925–2943; (*d*) J. Gu, W. Dong, Y. Tang, Y. Guo, L. Tang, J. Kong, S. Tadakamalla, B. Wang and Z. Guo, *J. Mater. Chem. C*, 2017, **5**, 6929–6936; (*e*) Y. Guo, G. Xu, X. Yang, K. Ruan, T. Ma, Q. Zhang, J. Gu, Y. Wu, H. Liu and Z. Guo, *J. Mater. Chem. C*, 2018, **6**, 3004–3015; (*f*) J. Lin, X. Chen, C. Chen, J. Hu, C. Zhou, X. Cai, W. Wang, C. Zheng, R. Zhang, J. Cheng, H. Liu and Z. Guo, *ACS Appl. Mater. Interfaces*, 2018, **10**, 6124–6136; (*g*) K. Sun, P. Xie, Z. Wang, T. Su, Q. Shao, J. Ryu, X. Zhang, J. Guo, A. Shankar, J. Li, R. Fan, D. Cao and Z. Guo, *Polymer*, 2017, **125**, 50–57; (*h*) X. Cui, G. Zhu, Y. Pan, Q. Shao, C. Zhao, M. Dong, Y. Zhang and Z. Guo, *Polymer*, 2018, **138**, 203–210; (*i*) X. Guo, S. Ge, J. Wang, X. Zhang, T. Zhang, J. Lin, C. X. Zhao, B. Wang, G. Fei and Z. Guo, *Polymer*, 2018, **143**, 155–163.
64 (*a*) B. Zhao, J. Deng, R. Zhang, L. Liang, B. Fan, Z. Bai, G. Shao and C. B. Park, *Eng. Sci.*, 2018, DOI: 10.30919/es8d735; (*b*) K. Zhang, G. Li, L. Feng, N. Wang, J. Guo, K. Sun, K. Yu, J. Zeng, T. Li, Z. Guo and M. Wang, *J. Mater. Chem. C*, 2017, **5**, 9359–9369; (*c*) P. Xie, Z. Wang, Z. Zhang, R. Fan, C. Cheng, H. Liu, Y. Liu, T. Li, C. Yan, N. Wang and Z. Guo, *J. Mater. Chem. C*, 2018, **6**, 5239–5249; (*d*) H. Wu, L. Jia, D. Yan, J. Gao, X. Zhang, P. Ren and Z. Li, *Compos. Sci. Technol.*, 2018, **156**, 87–94; (*e*) C. Luo, W. Duan, X. Yin and J. Kong, *J. Phys. Chem. C*, 2016, **120**, 18721–18732.
65 (*a*) Z. Hu, C. Wang and F. Zhao, *et al.*, *Nanoscale*, 2017, **9**, 8825; (*b*) Z. Hu, D. Zhang, L. Yu and Y. Huang, *J. Mater. Chem. B*, 2018, **6**, 518–526.